

# Computational Modeling of Gothic Microarchitecture

AVIV SEGALL, ETH Zurich, Switzerland

JING REN, ETH Zurich, Switzerland

MARTIN SCHWARZ, University of Basel, Switzerland

OLGA SORKINE-HORNUNG, ETH Zurich, Switzerland

Gothic microarchitecture is a design phenomenon widely observed in late medieval European art, comprising sculptural works that emulate the forms and structural composition of monumental Gothic architecture. Despite its prevalence in preserved artifacts, the design and construction methods of Gothic microarchitecture used by artisans remain a mystery, as these processes were orally transmitted and rarely documented. The Basel goldsmith drawings (“Basler Goldschmiedrisse”), a collection of over 200 late 15th-century design drawings from the Upper Rhine region, provide a rare glimpse into the workshop practices of Gothic artisans. This collection consists of unpaired 2D drawings, including top-view and side-view projections of Gothic microarchitecture, featuring nested curve networks without annotations or explicitly articulated design principles. Understanding these 2D drawings and reconstructing the 3D objects they represent has long posed a significant challenge due to the lack of documentation and the complexity of the designs. In this work, we propose a framework of simple yet expressive geometric principles to model Gothic microarchitecture as 3D curve networks, using limited input such as historical 2D drawings. Our approach formalizes a historically informed design space, constrained to tools traditionally available to artisans—namely compass and straightedge—and enables faithful reproduction of Gothic microarchitecture that conforms to physical artifacts. Our framework is intuitive and efficient, allowing users to interactively create 3D Gothic microarchitecture with minimal effort. It bridges the gap between historical artistry and modern computational design, while also shedding light on a lost chapter of Gothic craftsmanship.

CCS Concepts: • **Computing methodologies** → **Mesh models**.

Additional Key Words and Phrases: Gothic microarchitecture, surface modeling, curve networks, interactive editing

## ACM Reference Format:

Aviv Segall, Jing Ren, Martin Schwarz, and Olga Sorkine-Hornung. 2025. Computational Modeling of Gothic Microarchitecture. In *Special Interest Group on Computer Graphics and Interactive Techniques Conference Conference Papers (SIGGRAPH Conference Papers '25)*, August 10–14, 2025, Vancouver, BC, Canada. ACM, New York, NY, USA, 15 pages. <https://doi.org/10.1145/3721238.3730649>

## 1 Introduction

The term Gothic microarchitecture, as used by art historians, refers to a phenomenon widely observed in the design of late medieval European art: sculptural works that emulate the forms and structural composition of large-scale Gothic architecture [Bucher 1976].

Authors’ Contact Information: Aviv Segall, ETH Zurich, Switzerland, [aviv.segall@inf.ethz.ch](mailto:aviv.segall@inf.ethz.ch); Jing Ren, ETH Zurich, Switzerland, [jing.ren@inf.ethz.ch](mailto:jing.ren@inf.ethz.ch); Martin Schwarz, University of Basel, Switzerland, [martin.schwarz@unibas.ch](mailto:martin.schwarz@unibas.ch); Olga Sorkine-Hornung, ETH Zurich, Switzerland, [sorkine@inf.ethz.ch](mailto:sorkine@inf.ethz.ch).



This work is licensed under a Creative Commons Attribution 4.0 International License. *SIGGRAPH Conference Papers '25, Vancouver, BC, Canada*  
© 2025 Copyright held by the owner/author(s).  
ACM ISBN 979-8-4007-1540-2/2025/08  
<https://doi.org/10.1145/3721238.3730649>

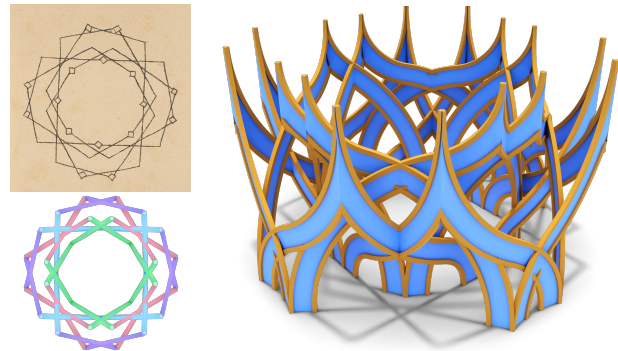


Fig. 1. *Top left*: Inv.U.XI.28 (10.4 × 15.3 cm). Image source: Kunstmuseum Basel (Public Domain). Basel goldsmith top-view drawing with reflectional and 4-fold rotational symmetries. *Right*: our reconstructed result with its top view shown on *bottom left* (the curve and its rotated or reflected replicas are shown in the same color).

This design phenomenon reached its apogee in the 15th century, particularly (if not exclusively) manifested in religious contexts, above all in church furnishings and liturgical objects (see Fig. 2). Formal features essential to Gothic monumental architecture—such as pointed and ogee arches, pinnacles, crockets, ribs and articulated profiles—permeated the full range of artifacts and miniature structures populating church spaces, including reliquaries, altar canopies, baldachins and sacrament houses, realized in wood, metal and stone [Binski 2014; Bork 2011; Kavalier 2012; Timmermann 2009]. Over the course of this period, Gothic microarchitecture grew increasingly ambitious and daring in its geometrizing design, eventually surpassing its architectural counterparts in structural complexity and formal innovation. One of the enduring, unsolved questions raised by the study of this phenomenon concerns the processes and methods of design practice. How did Gothic artisans, equipped with only a compass and a straightedge, conceive and develop these intricate creations?

The design and construction processes were never formally documented, but instead passed down through master-apprentice relationships, so that much of this knowledge has been lost [Bucher 1972]. Countless examples of Gothic microarchitecture are preserved in museums and churches, yet their original blueprints or construction plans have rarely survived. However, a singular exception is the corpus of late Gothic design drawings from the Upper Rhine region, known as the “Basler Goldschmiedrisse” (Basel goldsmith drawings) housed at the Kunstmuseum Basel [Falk 1979; Tanner 1991]. Dated to the end of the 15th century, this collection of over two hundred ink-on-paper drawings represents the most significant repository of such designs, both quantitatively and qualitatively. As such, they offer a rare window into the workshop of Gothic design,



Fig. 2. Microarchitectural superstructure of the main altarpiece at the church on mount Magdalensberg, Carinthia, Austria. Anonymous master of the elder Villach Workshop, 1502. Image credit: Wikimedia Commons, licensed under CC BY-SA 4.0.

presenting a unique opportunity to examine and reconstruct the fundamental procedures and geometrical operations that defined Gothic artistic practice [Burckhardt 1864; Ueberwasser 1930].

Of particular value for such an endeavor is a subgroup of the Basel drawings, comprising approximately seventy ground plans or top-view projections of microarchitectural elements (e.g., see Figures 1 and 4). Notably, and somewhat counter to modern intuition, these top-view schemes represent the initial stage of the Gothic design process. Starting with the ground plan allowed the designer to define the rotational and reflectional symmetries that shaped the overall structural configuration [Germund 1997; Müller 1990].

The next step in the design process involved generating a side view or elevation of the structure. Medieval German sources revealingly refer to this stage as “Auszug” (extraction process) [Shelby 1977]. This term denotes the extrusion of the design along the  $z$ -axis, yielding the side view of a given ground plan. However, the specifics of this step pose significant challenges to architectural historians. Certain geometry-based rules and formal constraints guided the translation of the ground plan into an elevation, but the few historical treatises in existence supply little information on the exact procedures [Bork 2014].

In this work, we make the first attempt to mathematically formulate the geometric principles underlying the extraction process. Our approach is based on the Basel corpus of drawings, as well as physical examples, allowing us to model Gothic microarchitecture from input 2D ground plans or top-view projections. The principles are grounded in traditional tools, such as the compass, and are designed to be generalizable to other historical artifacts. Our work illuminates the geometric principles underlying late Gothic design practices, making the Basel drawings comprehensible as 3D structures for the first time. Facilitating interactive and intuitive modeling, this also revives a sophisticated and historically significant design method, bringing it into the digital age. This effort holds great potential for art historians, designers and enthusiasts alike, advancing the study, restoration and creation of Gothic architecture.

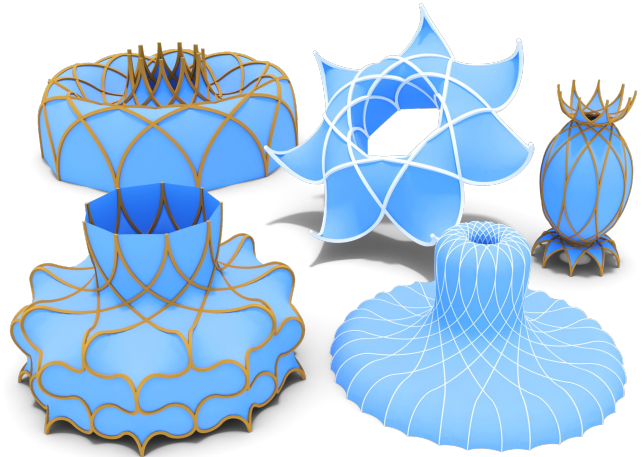


Fig. 3. Freeform design exploration using our user interface.

*Our contributions.* (1) We formulate the Gothic microarchitecture modeling problem as reconstructing 3D curve networks from given top-view projections, which may originate from digitized historical drawings or user-provided sketches. (2) We formalize the design space for Gothic microarchitecture, incorporating positional and tangential constraints to ensure that the side view resembles the ogee arches—an important characteristic we observe in historical drawings and physical artifacts. Our curve parameterization enables interactive editing in the side view while maintaining a fixed top view, ensuring that all edits remain within the defined design space. (3) We demonstrate that our method reliably and faithfully reproduces 3D Gothic microarchitecture from the Basel goldsmith drawings, maintaining consistency with the style and features of Gothic artistic products, as verified by art historians. (4) Our formulation can be interpreted as a simple yet expressive modeling language for curve-dominant architecture: using basic curves and specified symmetries, multi-layered and intricate structures can be created from a single drawing. This approach extends beyond modeling Gothic microarchitecture and can be applied in a broader context, such as free-form architectural design (see Fig. 3). Code and web demo for this paper are at [https://github.com/llorz/SIG25\\_goldschmiedrisse](https://github.com/llorz/SIG25_goldschmiedrisse).

## 2 Related work

*Biars.* A biarc consists of two *circular arcs* joined with  $G^1$  continuity, interpolating two input endpoints and their respective tangent directions while ensuring smooth transitions [Bolton 1975; Sandel 1937]. Biars are mathematically interesting as special cases of spirals with monotone piecewise continuous curvature [Kurnosenko 2009, 2013; Zwickler 2011]. Due to their simplicity and high precision in approximating smooth curves, biars find widespread applications across diverse fields such as computer graphics, architectural design and civil engineering. Notable uses include path planning with smooth transitions for CNC machines and robotic trajectories [Meeke and Walton 1992; Walton and Meeke 1994], structural stability in architectural arches [El-Mahdy 2014], shipbuilding [Bolton 1975], garment sewing pattern design [Ye et al. 2023], highway and railway alignment [Brustad and Dalmo 2020] and overflow spillway

design [Savage and Johnson 2001], to name a few. In the field of geometric modeling, much of the previous work has focused on fitting biarcs or curve splines to discrete data points [Meek and Walton 1992; Park 2004; Parkinson and Moreton 1991; Piegl and Tiller 2002; Schönherr 1993], or using biarcs to approximate Bézier segments [Walton and Meek 1994]. In this work, we use biarcs to parameterize the design space of Gothic microarchitecture.

*Ogee arcs & Gothic architecture.* Gothic architecture is most commonly associated with the pointed arch, valued both as a structural innovation and a decorative motif. Introduced at the turn of the 12th century, it revolutionized the structural engineering of vaulted spaces and became a ubiquitous element in the ornamentation of artifacts and architectural surfaces. In the 14th century, a new type of arch emerged: the double-curve arch known as the ogee (or *Kielbogen* in German, *acolade* in French). The ogee is a specialized form of a biarc, consisting of two circular arcs—typically with different radii—smoothly joined in opposite directions, creating a characteristic “S”-shape. While its origins can be traced to ancient Persian and Greek architecture [Boyd 1978], the ogee also appears in Islamic architecture and ornamental design [Rahman 2015], as well as in the Byzantine empire. It became a defining stylistic feature of the later Gothic period, gaining prominence during the 14th and, especially, the 15th century [Binski 2014]. Its convex-concave shape made it unsuitable for load-bearing purposes. “Strange, completely atectonic,” [Bucher 1976] the ogee’s attraction was aesthetic rather than structural: its dynamic and sensuous form—occasionally bending in three dimensions—charged it with ornamental expressiveness.

Existing scholarship has focused on the study of the Gothic ogee arc in its *planar* application, particularly in the design of window tracery. An important figure in the English Gothic revival movement, Billings [1851] made one of the first attempts to decipher the geometric principles behind Gothic window tracery, characterized by intricate 2D-patterns of circular arc segments, and included 100 detailed how-to drawings of various tracery designs. Most recently, Gfeller [2016] surveyed the Upper Rhine region’s rich heritage of late Gothic tracery and analyzed their geometric method of construction. Pioneering digital approaches enabled Gothic window tracery synthesis: Havemann and Fellner [2004] employed Generative Modeling Language to formalize the designs, combining basic geometric patterns into complex, customizable styles, while Takayama [2024] used metaballs [Ward 1999] to directly approximate motif shapes.

Geometric analysis of monumental architecture has a long history and increasingly employs digital tools, such as laser scanning, photogrammetry and CAD software, to extract and study the structural design of Gothic churches [Bork 2014, 2023; Tallon 2014]. Most recently, parametric 3D modeling has been leveraged for the analysis and virtual reconstruction of Gothic vaulting and spire construction and other architectural elements, yielding insight also into the procedural and generative nature of Gothic design techniques [Bereczki 2020, 2022, 2024]. Havemann and Fellner [2001] proposed a subdivision-based model representation for the reconstruction of cultural heritage sites, showcasing examples of Gothic architectural elements. However, their approach relies on user drawings and is not grounded in historical methodology. Notably, no comparable research exists in the field of Gothic microarchitecture.

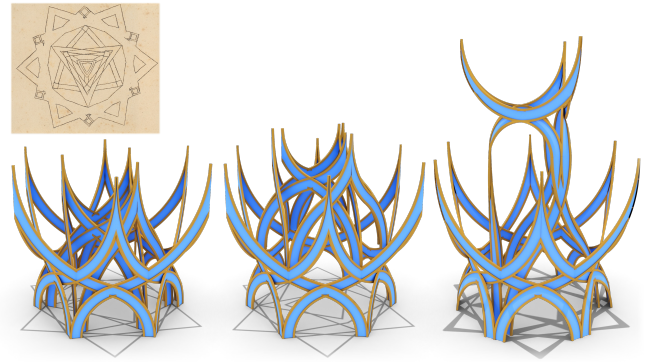


Fig. 4. Basel goldsmith drawings are top-view projections, which are inherently ambiguous. Here, we present three different Gothic-style reconstructions, all sharing the same top-view projections. *Top left:* Inv.U.XI.49 (10.2 × 14.6 cm). Image source: Kunstmuseum Basel (Public Domain).

*Curve networks*, consisting of feature curves, such as sharp edges, ridges, valleys and prongs, are essential for defining and revealing 3D shapes [Cole et al. 2008, 2009; Eissen and Steur 2007; Gal et al. 2009; Gehre et al. 2016; Gryaditskaya et al. 2019; Rivers et al. 2010; Saito and Takahashi 1990; Yoshizawa et al. 2005]. These networks are particularly significant in Gothic-style architecture where intricate, pointed curves define their unique character (see Fig. 2). Extensive research has focused on detecting feature curves on 3D shapes, facilitating a wide range of applications, including generating suggestive contours [DeCarlo et al. 2003; Gori et al. 2017; Hildebrandt et al. 2005], shape approximation or abstraction [De Goes et al. 2011; Mehra et al. 2009], shape reconstruction from incomplete data [Cao et al. 2016; Liu et al. 2008] and shape deformation via feature curves [Lai et al. 2006; Zhou et al. 2011]. Constructing meshes from curve networks is also actively studied [Bessmeltsev et al. 2012; Gryaditskaya et al. 2020; Hähnlein et al. 2022; Li et al. 2022; Orbay and Kara 2011; Pan et al. 2015; Yu et al. 2022], with an emphasis on aligning the resulting meshes to the flow-line directions defined by input designer curves. Additionally, sketch-based shape generation [Binninger et al. 2024; Guillard et al. 2021; Li et al. 2018; Nealen et al. 2007] contributes to this domain, leveraging user-drawn curves to create accurate and well-structured 3D models.

Among these efforts, Xu et al. [2014] and Gryaditskaya et al. [2020] address a problem similar to ours: reconstructing the 3D curve network from a single-view 2D input. Their approaches leverage *artistic priors*, such as common geometric regularities followed by designers [Xu et al. 2014], as well as additional straight-line scaffolds drawn by designers for structural support [Gryaditskaya et al. 2020]. These artistic priors provide critical guidance in their reconstruction process. However, Gothic-style curve networks present a more complex challenge, as the artistic priors underlying these intricate designs have largely been lost to history. Blueprints for Gothic-style microarchitecture are often only partially recorded in historical 2D drawings, typically as top-view projections, and lack corresponding side views. In this work, we address this gap by deriving geometric principles to reconstruct 3D curve networks using a novel parameterization, starting from these ambiguous 2D top-view drawings.

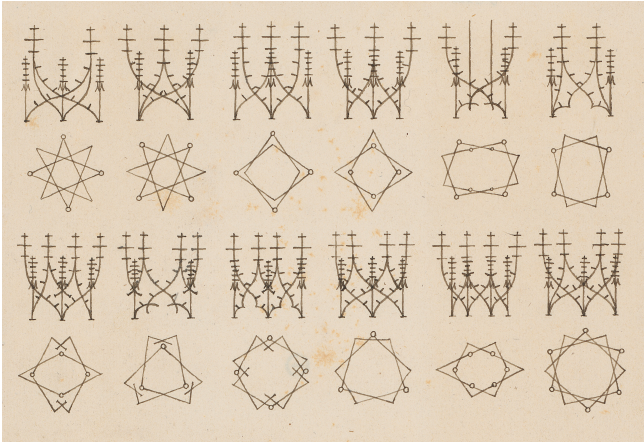


Fig. 5. Image: Inv.U.XI.11, ca. 1500, ink on paper, 19.8 × 30.2 cm. Source: Kunstmuseum Basel (Public Domain). This so-called *Lehrblatt* or teaching sheet may have served the instruction of apprentices in the workshop. For each top view drawing, shown in the 2nd and 4th rows, the corresponding front views are also illustrated.

### 3 Gothic microarchitecture

#### 3.1 Background

Grounded in the geometric procedures of Gothic architectural practice, the design of microarchitecture pushed these principles to new mathematical extremes. Unlike monumental structures, microarchitectural works were unconstrained by tectonic and material limitations. Their (much) smaller scale and non-load-bearing function afforded a greater degree of creative freedom, enabling the playful experimentation and virtuosic handling of geometric forms [Bucher 1976]. In contrast to monumental Gothic architecture, which has been the subject of extensive scholarly attention, the design process behind microarchitecture has been largely unstudied.

The Basel goldsmith drawings offer an excellent starting point for investigating the question of microarchitectural design practices. The complete corpus comprises over 200 drawings created by a single anonymous master, of which we focus on the 70 top-view plans that reveal a consistent design methodology. Each drawing represents a scaleless top-view projection, ranging from relatively simple to more complex linear or curvilinear schemes. Approximately half of these drawings depict what can be described as single-level structures, while the other half features multi-level designs. In these multi-level schemes, segments are stacked vertically, receding in a pyramidal formation (see Fig. 4 for an example). Collectively, they form something akin to a designer’s portfolio—a variegated set or toolbox of geometric modules, which could be employed in—and potentially adapted, customized and recombined for—specific projects [Huth 1923].

As noted in the introduction, the Basel drawings record only top views; no corresponding side views have survived, without which it is extremely difficult, if not impossible, to determine the intended 3D structures. The challenge is compounded by the lack of detailed historical information about the methods used to translate or extract these designs into volumetric forms. However, one exceptional drawing within the Basel corpus includes 12 paired top and side

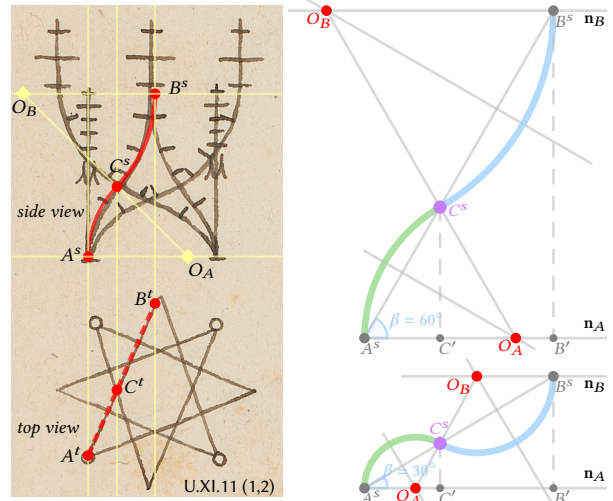


Fig. 6. *Left*: the second example from Fig. 5, highlighting one line in the top view and its corresponding side view in red. *Right*: two reconstructed side views from the same top view projection, using ogee arcs. The green and blue arcs meet at  $C^s$  with parallel tangents. Their centers ( $O_A$  and  $O_B$ ) lie along the normal directions of the endpoints ( $A^s$  and  $B^s$ ), denoted as  $n_A$  and  $n_B$ . See Sec. A in the supplementary materials for further discussion.

views (see Fig. 5). Referred to as the “*Lehrblatt*”, or teaching sheet, this drawing is believed to have served a pedagogical purpose within a workshop setting, illustrating the proper translation of exemplary top views into their corresponding side views.

#### 3.2 Observations & challenges

The teaching sheet shown in Fig. 5 serves as a kind of Rosetta Stone for our project. By reconstructing the relationship between the ground plan and elevation for each example and investigating physical Gothic microarchitecture, we make the following observations: (1) The Basel goldsmith drawings are *top-view* projections of 3D curve networks to be determined, showcasing prominent rotational and reflectional symmetries in different folds. (2) The *side view* of the curve networks in the main structure of Gothic microarchitecture conform to the ogee arch. (3) From the teaching sheet, we identify a crucial rule: the point where the curvature of the curve in the side view changes sign corresponds to an intersection point in the top view (see Fig. 6, left). Moreover, the tangents of the 3D curves at the endpoints are perpendicular to the floor plane, supporting the verticality characteristic of the Gothic style.

Therefore, to model Gothic microarchitecture, our goal is to compute the 3D curve networks that satisfy the following constraints: (1) **Positional constraints**: The top view of the 3D curves must align with the input 2D drawing, which can either be interactively created by users or digitally reconstructed from historical references. (2) **Tangential constraints**: The tangents of the 3D curves at the endpoints should be vertical. Additionally, for certain intersection points in the top view, the left and right tangents are supposed to be parallel (see Fig. 6, right).

The positional and tangential constraints define a design space for modeling Gothic microarchitecture. However, several challenges

remain to be addressed: (1) How can we mathematically define this design space, especially considering that the tangential constraints at the intersection points in the top view are somewhat ambiguous and not precisely defined? (2) How can we efficiently navigate this design space in a user-friendly manner? A straightforward approach might involve using Bézier curves to parameterize the 3D curve networks. However, during interactive modeling, when users adjust the positions or tangents of control points on the 3D curve, how to ensure that the updated curve continues to satisfy the constraints mentioned above and remains within the defined design space?

## 4 Methodology

Our method mirrors the historical extraction process (*Auszug*) based on the principles established in Sec. 3, enabling the computation of a set of 3D ogee curves from a given top-view projection. We first introduce the notations and review the definitions and properties of ogee arcs in Sec. 4.1. Next, we formally represent the input 2D top-view projection in Sec. 4.2. In Sec. 4.3, we present the geometric principles designed to estimate the height of points in the 2D side-view projection resembling an ogee arch, following the rules drawn from the teaching sheet. We then propose a new parameterization for a 3D curve based on both its top and side views in Sec. 4.4. Together, these steps enable the reconstruction of a 3D curve network from the input top-view projection while allowing for interactive and intuitive editing within the design space of Gothic microarchitecture, ensuring that one view remains unchanged when editing the other.

### 4.1 Notations & preliminaries

An arbitrary curve  $\ell$  connecting two points  $A$  and  $B$  is denoted by  $\ell = \overline{AB}$ . In particular,  $\overline{AB}$  denotes a *line segment*, while  $\widehat{AB}$  represents a *circular arc* connecting the points  $A$  and  $B$ . For a point  $X$ , we represent its embedded position in 2D or 3D using bold font,  $\mathbf{X}$ . We use the subscripts  $t$  or  $s$  to refer to points in the top view or side view, respectively. A *biarc* consists of two circular arcs joined with  $G^1$ -continuity, meaning that the tangents at the common point are colinear. We focus on a subset of biarcs where the curvatures at the common point of the two circular arcs have *opposite signs*. This configuration is exemplified by the classic *ogee arcs* in architecture and the *reverse curve* in civil engineering:

*Definition 4.1.* Given two points  $A$  and  $B$  with tangents  $\mathbf{d}_A$  and  $\mathbf{d}_B$ , a **reverse curve** is a pair of circular arcs  $\widehat{AC}$  and  $\widehat{CB}$  that connect  $A$  and  $B$  while maintaining the specified tangents. The arcs turn in opposite directions and share a common tangent line at their intersection,  $C$ , known as the **Point of Reverse Curvature (PRC)**.

A reverse curve can be defined by five control points: the two given endpoints and three to-be-determined points, which include the centers of the two circles and the intersection point (PRC). The reverse curve that interpolates the input endpoints with specified tangents is *not* unique, it has one degree of freedom. To ensure uniqueness, an additional constraint is required, such as minimizing the difference in the radii of the two circular arcs [Bolton 1975; Park 2004]. Sandel [1937] demonstrates that the *locus* of all feasible PRCs for a given pair of points and their specified tangents forms a circular arc connecting the two points. In the special case where the tangents are parallel, this locus reduces to the line segment

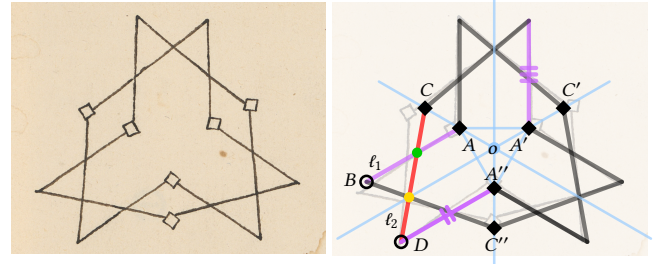


Fig. 7. *Left:* Inv.U.XI.18, 10.5 × 15.2 cm. Image source: Kunstmuseum Basel (Public Domain). This drawing can be represented as  $\mathcal{D} = \{\ell_1 \cup \ell_2, C_3(o), \sigma_y\}$ , including two basic curves  $\ell_1 = \overline{AB}$  and  $\ell_2 = \overline{CD}$  (colored in purple and red resp.), exhibiting 3-fold rotational symmetry about point  $o$  (denoted as  $C_3(o)$ ) and reflection symmetry along  $y$ -axis (denoted as  $\sigma_y$ ).

connecting the two points. As the original proof is presented in German, we include a complete derivation of these results in the supplementary material Sec. A for completeness.

**REMARK 1.** Given two points  $A$  and  $B$  with **parallel tangents**  $\mathbf{d}_A \parallel \mathbf{d}_B$ , the point of reverse curvature (PRC) of any reverse curve connecting  $A$  and  $B$  lies on  $\overline{AB}$ , i.e., the line segment joining  $A$  and  $B$ .

### 4.2 Top view representation

The top-view orthographic projections of the Basel drawings are governed by symmetry. To represent this, we use a set of symmetric 2D curves, such as the one shown in Fig. 7. Specifically, we define the top view as  $\mathcal{D}^t = \{\mathcal{L}^t, C_n(\mathbf{p}), \sigma_{\mathbf{d}}\}$ , where  $\mathcal{L}^t$  is a set of *distinct* 2D curves, meaning that no two curves in  $\mathcal{L}^t$  can be obtained from one another through symmetry transformations. Here,  $C_n(\mathbf{p})$  denotes  $n$ -fold rotational symmetry about the point  $\mathbf{p}$ , and  $\sigma_{\mathbf{d}}$  represents reflectional symmetry through the axis  $\mathbf{d}$ . The complete set  $\mathcal{D}^t$  is generated by applying a set of roto-reflection operators  $\{\mathbf{R}^k \mathbf{Q}^r \mid k = 1, \dots, n; r = 0, 1\}$ , where  $\mathbf{R}$  is a rotation matrix about  $\mathbf{p}$  by  $\frac{360^\circ}{n}$ , and  $\mathbf{Q}$  is a reflection matrix through axis  $\mathbf{d}$ . Each curve  $\ell \in \mathcal{L}^t$  is referred to as a *basic curve*, while any other curve  $\ell' \in \mathcal{D}^t$  that has the same shape as  $\ell$  is considered a *replica*, obtained through rotation or reflection. Note that a top-view drawing may contain multiple basic curves, i.e.,  $\mathcal{L}^t = \ell_1^t \cup \dots \cup \ell_k^t$  (see Fig. 7) or simply a single one (see Fig. 6). Recall that we assume the top view is provided as input, either by the user or from historical drawings, meaning that the parameterized curves  $\mathcal{L}^t$  are already known.

### 4.3 Side view reconstruction

Drawing from the side-view sketches in the teaching notes, we first formally define the side-view projection as the orthographic projection of the 3D curve network onto a vertical plane (perpendicular to the floor plane) that contains a reflectional axis from the top-view projection. We start from the simplest case where the input top-view projection only has one basic curve, see Fig. 6 (left) as an example: we highlight the basic curve in its top view and side view in red and make the following observations:

- (1) Vertices marked as circles (Fig. 5) or diamonds (Fig. 7) in the top view are positioned on the ground floor, i.e., at zero height in

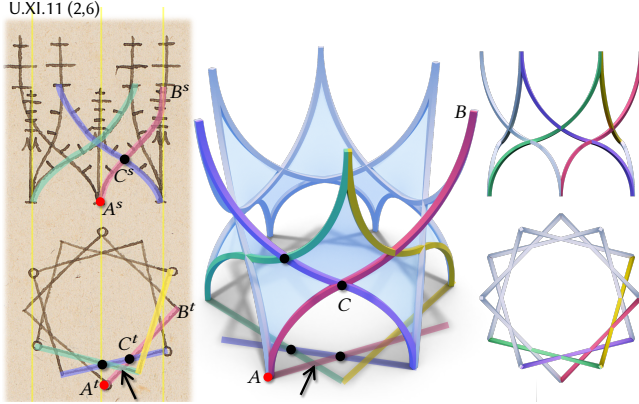


Fig. 8. *Left*: the last example from Fig. 5. *Right*: our reconstruction in three views. Four curves are highlighted in consistent colors. Notably, the turquoise and red curves appear to intersect in the top view but remain distinct in 3D.

the side view. For instance, in Fig. 8, point  $A^t$  is marked as a circle in the top view, and its side view  $A^s$  lies on the ground.

- (2) The endpoints of the basic curve exhibit vertical tangents (perpendicular to the ground) in the side view, see the tangents at points  $A^s$  and  $B^s$  in Figures 6 and 8.
- (3) The side view of a basic curve resembles a reverse curve, where the PRC—the point at which the curvature changes sign (see the point  $C^s$  in Fig. 8 top left)—corresponds to an intersection point in the top view (i.e., the point  $C^t$  in Fig. 8 bottom left).

These observations may seem straightforward to formulate at first glance, but they raise a critical question: in the top-view projection, where multiple intersection points exist between the basic curve and its replicas, how can we identify the PRC for the ogee arc? For example, Fig. 8 (right) shows our reconstructed 3D curve network for one example from the teaching sheet, with four 3D curves, and its corresponding top- or side-view projections highlighted in the same color. We observe that although the turquoise curve and the red curve intersect in the top view (marked with an arrow), they do not intersect in 3D. We define an intersection point in the top view as a *true* intersection if the corresponding curves also intersect in 3D; otherwise, we refer to it as a *false* intersection. For the basic curve (e.g., the purple curve), its top-view projection can have multiple true intersections. Therefore, we must decide which true intersection in the top view corresponds to the PRC in the side view.

**4.3.1 Determining the PRC.** We begin by addressing how to disambiguate true intersections from false intersections in the top view. Given a basic curve  $\ell(t)$  with parameter  $t$ , and its replica  $\ell'(t')$  with parameter  $t'$ , an intersection point in the top view is considered a true intersection if and only if the parameters of the curves at the intersection satisfy  $t = t'$ . The condition arises from two facts: first, the height function of a basic curve is monotonically increasing (as shown in the side-view projection in the teaching sheet). Second, its reflected or rotated replicas (as specified from the input top-view) share the same height function. Therefore, the intersection in the top view is a true intersection if and only if the corresponding points of the two curves have the same height, i.e., satisfying  $t = t'$ . In this

way, we can easily distinguish true intersections from false intersections between the basic curve and its replicas (as shown in Fig. 8). For example, in Fig. 7 the yellow point is a true intersection, since  $\overline{C''B}$  is a replica of  $\overline{CD}$  and they intersect at identical parameter values along their lengths (as the intersection lies on the blue reflective axis). It is important to note that the intersection between two different basic curves (e.g., the green point in Fig. 7, left) can always be a true intersection. This is because the two curves have independent parameters and distinct height functions, and their intersection in 3D inherently has a valid solution. From the teaching sheet and physical objects, we observe that the side view of each basic curve has one point of reverse curvature. When multiple true intersections occur in the top view, the point closest to the midpoint is typically selected as the PRC, resulting in a more balanced ogee arc. See detailed discussions in Algo. 1 in supplemental Sec. C.

**4.3.2 Fitting biarcs to the side views.** For any basic curve  $\widetilde{AB} \in \mathcal{L}^t$  we have identified its point of reverse curvature (PRC), denoted as the point  $C$ . Our goal is now to determine the height of the three points  $A$ ,  $B$ , and  $C$  such that a biarc can be fitted through them. By combining this height information with their given top-view projection, we can reconstruct the 3D curve. As noted above, additional marks such as circles or diamonds indicate that the vertices with these marks have a height of zero. According to Remark 1, the heights of points  $B$  and  $C$  are interdependent, with one degree of freedom. Specifically, assuming the tangents at the two endpoints  $A$  and  $B$  are perpendicular to the floor plane, the locus of the PRC for all biarcs connecting  $A$  and  $B$  lies along the line segment connecting these two points. Therefore, if the height of point  $B$  is fixed, the height of point  $C$  can be determined as the intersection of the line segment  $\overline{A^sB^s}$  with the vertical line passing through the top-view projection of  $C^t$ . By assigning different heights to point  $B$ , we can derive biarcs of varying shapes, see Fig. 6 (right) for two examples. Similarly, if the height of the PRC point  $C$  is known, the height of the point  $B$  can be determined as the intersection of the line passing through  $A^s$  and  $C^s$  with the vertical line passing through the top-view projection of  $B^t$ . This approach allows us to derive the side-view projection from the top-view projection. In other words, for any point in the top-view projection, its height can be computed to determine its 3D position.

#### 4.4 3D curve parameterization

Instead of directly parameterizing a 3D curve  $\ell = \widetilde{AB}$ , we propose a novel parameterization defined by its top view  $\ell^t = \widetilde{A^tB^t}$  and side view  $\ell^s = \widetilde{A^sB^s}$ . Given the top-view 2D curve parameterized as

$$\ell^t(u) = (x(u), y(u))^T, \quad u \in [0, 1] \quad \text{s.t.} \quad \ell^t(0) = A^t, \quad \ell^t(1) = B^t,$$

where  $A^t$  and  $B^t$  are the 2D positions of points  $A$  and  $B$  from the top view, and given the side-view 2D curve parameterized as

$$\ell^s(v) = (g(v), h(v))^T, \quad v \in [0, 1] \quad \text{s.t.} \quad \ell^s(0) = A^s, \quad \ell^s(1) = B^s,$$

where  $A^s$  and  $B^s$  are the 2D positions of points  $A$  and  $B$  projected onto the side-view vertical plane, we can now reconstruct the 3D curve  $\ell(u)$  from the top view  $\ell^t(u)$  and side view  $\ell^s(v)$ :

$$\ell(u) = (x(u), y(u), h(g^{-1}(p(u))))^T, \quad (1)$$

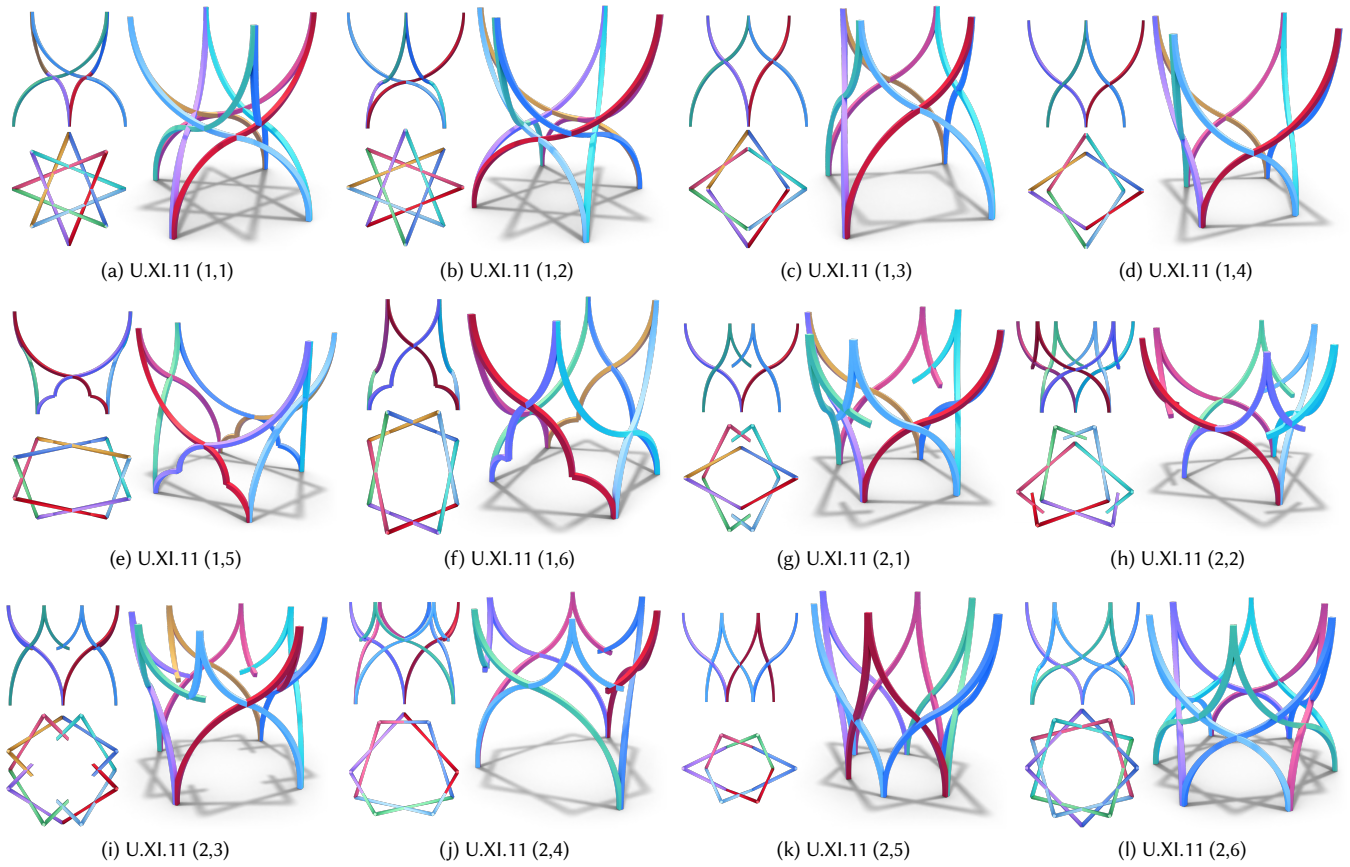


Fig. 9. For the example in  $i$ -th row,  $j$ -th column in the teaching sheet shown in Fig. 5, we show our reconstructed results in the sub-figure U.XI.11 ( $i,j$ ), in three different views: the 3D view is rendered using a perspective camera, while the 2D top and side views are rendered using orthographic camera.

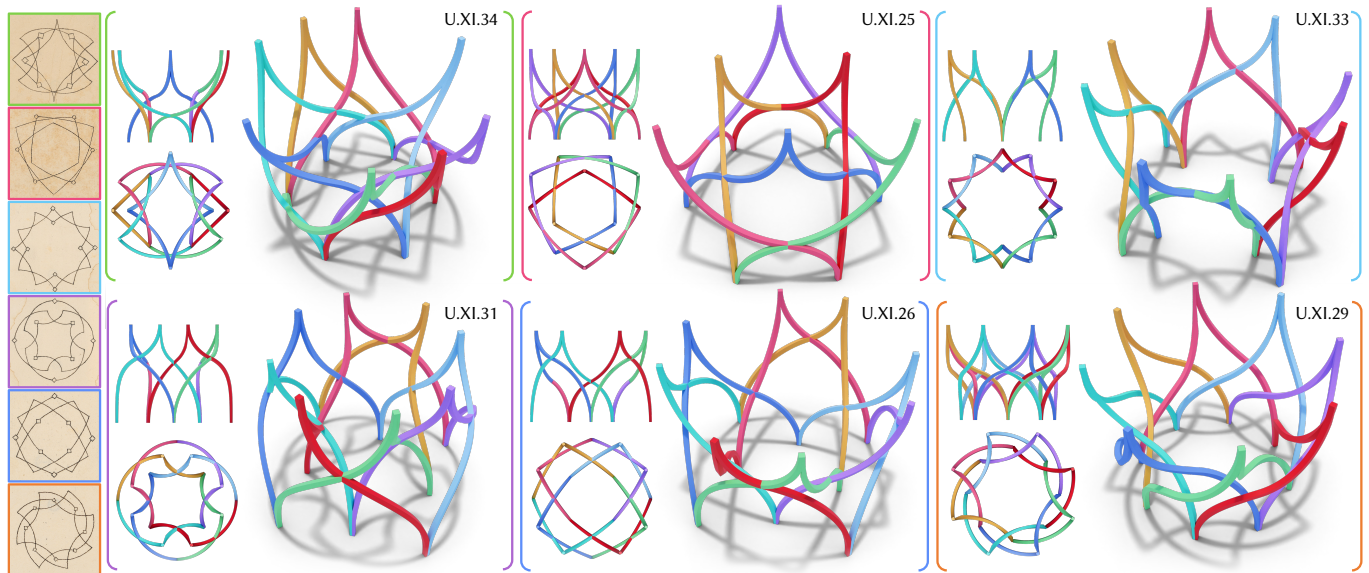


Fig. 10. Basel goldsmith drawings showcasing 2-,3-4- and 8-fold rotational symmetry with *curved* basic curves. The reconstructed results are presented from three different views. Image source for the Basel goldsmith drawings shown on the left: Kunstmuseum Basel (Public Domain).

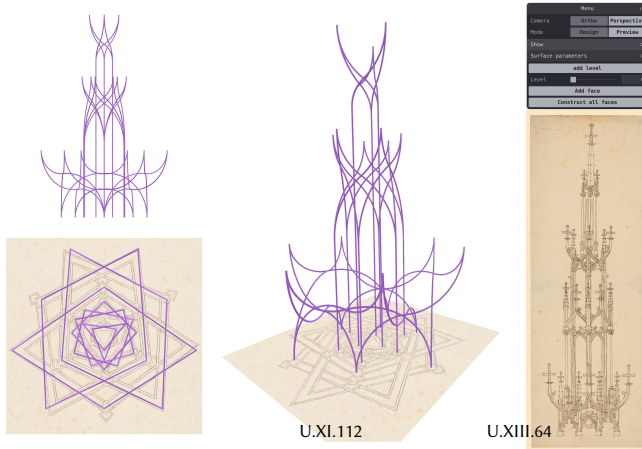


Fig. 11. Screenshot of our web-based user interface: The (unrelated) side-view drawing (Inv.U.XIII.64, 41.1 × 14.1 cm) is used as a reference to reconstruct the top-view drawing (Inv.U.XI.112, 21 × 29.9 cm) featuring a multi-layer structure. Image source: Kunstmuseum Basel (Public Domain).

where  $p(u)$  is a function that captures the dependency between variables  $u$  and  $v$ , i.e.,  $p(u) = g(v)$ . One natural choice for  $p(\cdot)$  is an orthographic projection onto the side-view vertical plane inclined at an angle  $\theta$  to the  $x$ -axis, yielding  $p(u) = x(u) \cos \theta + y(u) \sin \theta$  (see Fig. A.3 in the supplementary for a geometric interpretation). Alternatively, to achieve a reconstruction that is independent of both the side-view direction and the top-view parameterization,  $p(u)$  can be defined as the arc length of the top-view curve:  $p(u) = \int_0^u \sqrt{x'(t)^2 + y'(t)^2} dt$ . For simpler implementations, the choice  $p(u) = u$  also ensures side-view independence. See Sec. B in the supplementary for a detailed derivation. Unlike the standard parameterization, which uses the same parameter to parameterize the  $x, y, z$ -coordinate functions, our new parameterization, defined in Eq. (1), uses four functions  $x(u), y(u), g(v), h(v)$  defined by two dependent variables  $u, v$ . This parameterization allows us to modify the shape of the curve in one view while keeping the other view unchanged.

## 5 Results

We developed a web-based user interface (see Figures 11 and 12) for interactive modeling in JavaScript. Our UI supports top-view drawing and editing of lines and arcs, side-view auto-generation and editing, multi-layer drawings and various visualizations for curves and faces. Please refer to the accompanying video and Sec. C in the supplementary material for more details.

The geometric principles derived from a single example in the teaching sheet, specifically Fig. 6, can be applied to the other examples as well. Fig. 9 shows our reconstructed results, where the side views and top views are in precise alignment with the drawings in the teaching sheet shown in Fig. 5. These principles can also be effectively generalized to all other top-view drawings in the Basel goldsmith collection that lack corresponding side views. Fig. 1 shows an example with a complex structure containing four unique basic curves. Fig. 4 shows an example with a multi-layered structure exhibiting a combination of 3-fold and 6-fold symmetries. Fig. 10 shows six examples with different symmetries, featuring

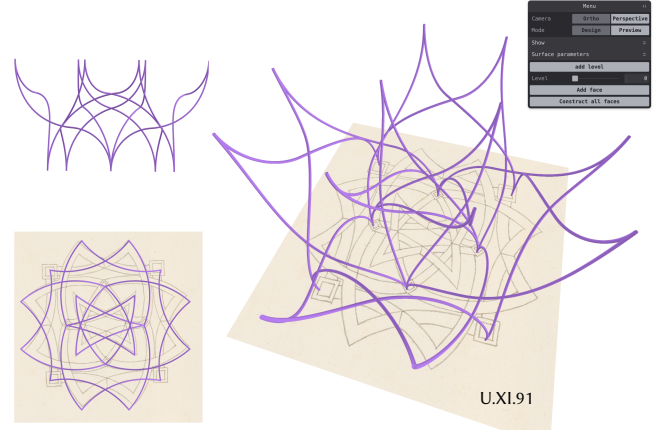


Fig. 12. Screenshot of our web-based user interface. With fewer than ten clicks, users can easily recreate the historical drawing. Our reconstruction, colored in purple, is displayed from three different perspectives. Image: Inv.U.XI.91, 15.1 × 20.7 cm. Source: Kunstmuseum Basel (Public Domain).

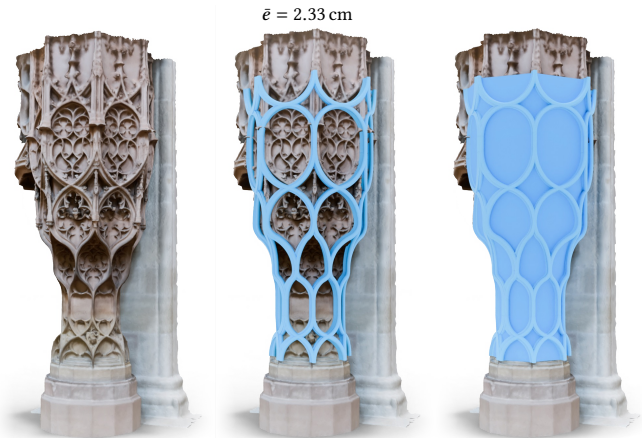


Fig. 13. A 3D scan of the late Gothic chancel, measuring 385 cm in height, by Hans Nussdorf (1486) in the Basel Minster featuring a 7-fold rotational symmetry. We show our reconstructed object in blue and report its RMSE ( $\bar{\epsilon}$ ) to the reference scan. Note that the error is only measured on the front half, as the scan is incomplete.

nonlinear basic curves in the top view drawings. Since no ground-truth side views or corresponding 3D objects are known to exist, we cannot quantitatively evaluate the accuracy of our reconstruction of Basel goldsmith drawings. However, domain experts have found our reconstructed results plausible and valuable. The results were shared with select experts in Gothic drawing and design at the Kunstmuseum Basel<sup>1</sup> and the Metropolitan Museum of Art in New York<sup>2</sup>, as well as with architectural historians<sup>3</sup>. Their feedback confirmed 1) the general plausibility of the reconstructions, 2) the scholarly importance of unlocking this archive of designs for further study and 3) the innovative nature of the methodology, which may

<sup>1</sup>Ariane Mensger, Kunstmuseum Basel, ariane.mensger@bs.ch

<sup>2</sup>Femke Speelberg, Metropolitan Museum of Art, Femke.Speelberg@metmuseum.org

<sup>3</sup>Robert Bork, University of Iowa, robert-bork@uiowa.edu



Fig. 14. Reconstruction based on *side views* of physical objects (a-c) or prints (d-f). Image sources: (a-c) Wikimedia Commons (CC BY-SA 4.0); (d) Inv.49.97.607a, (57.6 × 12.1 cm), The Metropolitan Museums of Art (Public Domain); (e) Inv.E.1.124 (68.6 × 13.2 cm), ©The Trustees of the British Museum (CC BY-NC-SA 4.0); (f) doi:10.11588/digit.34056, Heidelberg University Digital Library (Public Domain).

be adapted and expanded to other geometry-dominated aspects of Gothic architecture.

Our method also simplifies modeling Gothic microarchitecture from partial side views. Users can estimate the structure’s symmetry group, determine or approximate the depth differences between layers, and then use our UI to create the model. For example, we use our interactive design tool to digitally reconstruct a Gothic chancel from its side view (see Fig. 13). The resulting model aligns precisely with the 3D scan. Fig. 14 shows more reconstruction results from partial side views of Gothic microarchitecture, using photos or prints as references. In two or three iterations, we managed to get accurate reconstructions that match the references.

Our formulation is intuitive and effective, with most results requiring fewer than ten clicks in our UI. This ease of use enables non-technical experts, such as architectural historians, to employ this tool in their research or in the classroom. Our formulation can also be interpreted as a simple yet expressive modeling language for curve-dominant freeform design. Drawing just one or two distinct curves, users can create a complicated structure as demonstrated in Fig. 3, where the boundaries of the faces are automatically detected and filled with a minimal-area surface [Pinkall and Polthier 1993]. This approach enables effortless exploration of symmetric shapes with minimal effort. Fig. 15 shows another example of using our user interface to easily replicate an architectural design.

## 6 Conclusion, limitations & future work

Our project deciphers a Gothic design space through a specially deduced set of geometric rules and a 3D curve parameterization suited to this task. This tool benefits both scholars and designers by unlocking new insights into Gothic microarchitecture. For art historians, the 3D modeling of the Basel *Goldschmiedrisse* reveals their encoded structures, making these designs accessible for further study. It enables systematic matching of specific drawings to surviving Gothic works and facilitates the reverse-engineering of

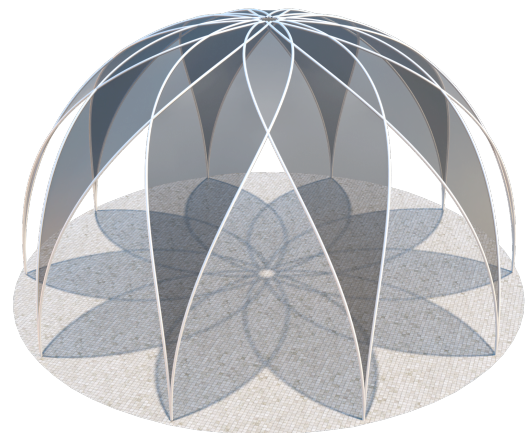


Fig. 15. Inspired by “The Peace Tent” built in Kazakhstan [VDS 2019], we create a digital replica using our UI with less than five clicks.

their geometric structure. More fundamentally, our design space demonstrates how elaborate 3D curve-networks emerge from deceptively simple 2D line drawings. By aligning our perspective with the methods of Gothic artists, it unveils the rational geometric order that underpins these fantastical, mathematical forms, allowing us to see through the eyes of their creators. Additionally, it can serve as a powerful pedagogical tool, introducing students of art and design to pre-digital parametric design methods that differ fundamentally from the dominant classical architectural tradition, but hold a surprising kinship with contemporary digital trends in architectural practice.

Our project facilitates not only the reconstruction and study of historical objects but also a digital revival of Gothic-inspired design practice. By mathematically formulating the underlying geometric principles, we significantly reduce the complexity of digitally

modeling Gothic microarchitecture. This advancement holds great potential for various applications. In the game industry, where intricate and historically accurate designs are often needed but demand substantial artist input, our approach can streamline the creation process. Similarly, it can advance object and building reconstruction within the fields of computer graphics and computer vision, providing a more efficient and precise methodology for recreating complex architectural forms.

Our algorithm has some limitations. While our formulation allows the height of the Gothic microarchitecture to be freely adjusted—decoupled from its ground plan proportions—this design flexibility can diverge from historically rule-bound practices (which themselves varied across regions and time periods). Currently, the algorithm does not account for vertical pinnacles and second-order ornaments (such as crockets). Further, it only supports creating a single object of Gothic microarchitecture with multiple layers, while many physical objects contain multiple decorations, each consisting of its own multilayered Gothic microarchitecture. In future work, we aim to explore the principles for assembling Gothic ornaments into complete designs. It would also be interesting to design algorithms capable of automatically synthesizing faithful Gothic microarchitecture without user input.

## Acknowledgments

The authors express gratitude to the anonymous reviewers for their valuable feedback. The authors are deeply grateful to the Kunstmuseum Basel, especially to Ariane Mensger, for facilitating access to study the drawings in person. Special thanks to Ningfeng Zhou for proofreading and to Marcel Padilla for his spiritual guidance. The authors also extend their thanks to all IGL members for the discussions and support. This work was supported in part by the ERC Consolidator Grant No. 101003104 (MYCLOTH).

## References

- Zoltán Bereczki. 2020. Generative Interpretations of Late Gothic Architectural Forms. *Symmetry: Culture and Science* 31 (01 2020), 279–295.
- Zoltán Bereczki. 2022. Order, Procedure, and Configuration in Gothic Architecture: A Case Study of the Avas Church, Miskolc, Hungary. *Architecture* 2, 4 (2022), 671–689.
- Zoltán Bereczki. 2024. Gótikus mikroarchitektúrális alkotások 3d szkenelésének módszerei és problémái. *Multidiszciplináris Tudományok* 14 (10 2024), 310–322. <https://doi.org/10.35925/j.multi.2024.4.26>
- Mikhail Bessmeltsev, Caoyu Wang, Alla Sheffer, and Karan Singh. 2012. Design-driven quadrangulation of closed 3D curves. *ACM Trans. Graph.* 31, 6 (2012), 178–1.
- Robert William Billings. 1851. *The Power of Form Applied to Geometric Tracery: One Hundred Designs and Their Foundations Resulting from One Diagram*. W. Blackwood and sons, UK.
- Alexandre Binniger, Amir Hertz, Olga Sorkine-Hornung, Daniel Cohen-Or, and Raja Giryes. 2024. SENS: Part-Aware Sketch-based Implicit Neural Shape Modeling. *Computer Graphics Forum (Proceedings of EUROGRAPHICS 2024)* 43, 2 (2024), 1–14.
- Paul Binski. 2014. *Gothic Wonder: Art, Artifice and the Decorated Style 1290–1350*. Yale University Press.
- KM Bolton. 1975. Biarcs curves. *Computer Aided Design* 7, 2 (1975), 89–92.
- Robert Bork. 2014. Dynamic unfolding and the conventions of procedure: Geometric proportioning strategies in Gothic architectural design. *Architectural Histories* 2, 1 (2014), 1–20.
- Robert Bork. 2023. *Designing the Regensburg Spire and Harburg Tabernacle: The Geometries of Two Great German Gothic Drawings*. Amsterdam University Press, 15–40.
- Robert Odell Bork. 2011. *The geometry of creation: architectural drawing and the dynamics of gothic design*. Ashgate Publishing, Ltd., UK.
- Thomas D Boyd. 1978. The arch and the vault in Greek architecture. *American Journal of Archaeology* 82, 1 (1978), 83–100.
- Tanita Fossli Brustad and Rune Dalmo. 2020. Railway transition curves: a review of the state-of-the-art and future research. *Infrastructures* 5, 5 (2020), 43.
- François Bucher. 1972. Medieval architectural design methods, 800-1560. *Gesta* 11, 2 (1972), 37–51.
- François Bucher. 1976. Micro-architecture as the 'idea' of Gothic Theory and Style. *Gesta* 15, 1/2 (1976), 71–89.
- Jacob Burckhardt. 1864. Über die Goldschmiedrisse der öffentlichen Kunstsammlung zu Basel. *Basler Taschenbuch* 12 (1864), 99–122.
- Yuanhao Cao, Liangliang Nan, and Peter Wonka. 2016. Curve networks for surface reconstruction. *arXiv preprint arXiv:1603.08753* (2016), 1–8.
- Forrester Cole, Aleksey Golovinskiy, Alex Limpaecher, Heather Stoddart Barros, Adam Finkelstein, Thomas Funkhouser, and Szymon Rusinkiewicz. 2008. Where do people draw lines? *ACM Trans. Graph.* 27, 3 (2008), 88:1–11.
- Forrester Cole, Kevin Sanik, Doug DeCarlo, Adam Finkelstein, Thomas Funkhouser, Szymon Rusinkiewicz, and Manish Singh. 2009. How well do line drawings depict shape? *ACM Trans. Graph.* 28, 3 (2009), 28:1–9.
- Fernando De Goes, Siome Goldenstein, Mathieu Desbrun, and Luiz Velho. 2011. Exoskeleton: Curve network abstraction for 3d shapes. *Computers & Graphics* 35, 1 (2011), 112–121.
- Doug DeCarlo, Adam Finkelstein, Szymon Rusinkiewicz, and Anthony Santella. 2003. Suggestive contours for conveying shape. *ACM Trans. Graph.* 22, 3 (July 2003), 848–855. <https://doi.org/10.1145/882262.882354>
- Koos Eissen and Roselien Steur. 2007. *Sketching, drawing techniques for product designers*. BIS publishers, Netherlands.
- Ghada M El-Mahdy. 2014. Parametric study of the structural and in-plane buckling analysis of ogee arches. *HBRC Journal* 10, 1 (2014), 108–116.
- Tilman Falk. 1979. *Katalog der Zeichnungen des 15. und 16. Jahrhunderts im Kupferstichkabinett Basel*. Vol. 1. Schwabe, Basel, Switzerland.
- Ran Gal, Olga Sorkine, Niloy J Mitra, and Daniel Cohen-Or. 2009. iWIRES: An analyze-and-edit approach to shape manipulation. *ACM Trans. Graph.* (2009), 1–10.
- Anne Gehre, Isaak Lim, and Leif Kobbelt. 2016. Adapting feature curve networks to a prescribed scale. *Computer graphics forum* 35, 2 (2016), 319–330.
- Ute Germund. 1997. *Konstruktion und Dekoration als Gestaltungsprinzipien im spätgotischen Kirchenbau: Untersuchungen zur mittelrheinischen Sakralbaukunst*. Werner.
- Walter Gfeller. 2016. *Geschichte des Masswerks am Oberrhein: die Eingebung des entwerfenden Baumeisters und ihre geometrische Funktion*. Michael Imhof.
- Giorgio Gori, Alla Sheffer, Nicholas Vining, Enrique Rosales, Nathan Carr, and Tao Ju. 2017. FlowRep: Descriptive Curve Networks for Free-Form Design Shapes. *ACM Trans. Graph.* 36, 4 (2017), 59:1–14. <https://doi.org/10.1145/3072959.3073639>
- Yulia Gryaditskaya, Felix Hähnlein, Chenxi Liu, Alla Sheffer, and Adrien Bousseau. 2020. Lifting Freehand Concept Sketches into 3D. *ACM Trans. Graph.* 39, 6 (2020), 167:1–16.
- Yulia Gryaditskaya, Mark Sypsteyn, Jan Willem Hoftijzer, Sylvia C Pont, Frédo Durand, and Adrien Bousseau. 2019. OpenSketch: a richly-annotated dataset of product design sketches. *ACM Trans. Graph.* 38, 6 (2019), 232–1.
- Benoit Guillard, Edoardo Remelli, Pierre Yvermay, and Pascal Fua. 2021. Sketch2mesh: Reconstructing and editing 3d shapes from sketches. In *Proceedings of the IEEE/CVF International Conference on Computer Vision*. Montreal, QC, Canada, 13023–13032.
- Felix Hähnlein, Yulia Gryaditskaya, Alla Sheffer, and Adrien Bousseau. 2022. Symmetry-driven 3D reconstruction from concept sketches. In *ACM SIGGRAPH 2022 Conference Proceedings*. 1–8.
- Sven Havemann and Dieter Fellner. 2001. A versatile 3d model representation for cultural reconstruction. In *Proceedings of the 2001 conference on Virtual reality, archeology, and cultural heritage*. ACM, New York, NY, USA, 205–212.
- Sven Havemann and Dieter Fellner. 2004. Generative parametric design of gothic window tracery. In *Proceedings Shape Modeling Applications*. USA, 350–353.
- Klaus Hildebrandt, Konrad Polthier, and Max Wardetzky. 2005. Smooth Feature Lines on Surface Meshes. In *Symposium on geometry processing*. Eurographics Association, Netherlands, 85–90.
- Hans Huth. 1923. *Künstler und Werkstatt der Spätgotik*. Filser.
- Ethan Matt Kavaler. 2012. *Renaissance Gothic: architecture and the arts in northern Europe 1470-1540*. Yale University Press, USA.
- Alexey Kurnosenko. 2009. General properties of spiral plane curves. *Journal of Mathematical Sciences* 161, 3 (2009), 1–8.
- Alexey Kurnosenko. 2013. Biarcs and bilens. *Computer Aided Geometric Design* 30, 3 (2013), 310–330.
- Yu-Kun Lai, Qian-Yi Zhou, Shi-Min Hu, Johannes Wallner, and Helmut Pottmann. 2006. Robust feature classification and editing. *IEEE Transactions on Visualization and Computer Graphics* 13, 1 (2006), 34–45.
- Changjian Li, Hao Pan, Adrien Bousseau, and Niloy J Mitra. 2022. Free2cad: Parsing freehand drawings into cad commands. *ACM Trans. Graph.* 41, 4 (2022), 1–16.
- Changjian Li, Hao Pan, Yang Liu, Xin Tong, Alla Sheffer, and Wenping Wang. 2018. Robust flow-guided neural prediction for sketch-based freeform surface modeling. *ACM Trans. Graph.* 37, 6 (2018), 1–12.
- Lu Liu, Chandrajit Bajaj, Joseph O Deasy, Daniel A Low, and Tao Ju. 2008. Surface reconstruction from non-parallel curve networks. *Computer Graphics Forum* 27, 2 (2008), 155–163.
- Derek S Meek and Desmond J Walton. 1992. Approximation of discrete data by G1 arc splines. *Computer Aided Design* 24, 6 (1992), 301–306.

- Ravish Mehra, Qingnan Zhou, Jeremy Long, Alla Sheffer, Amy Gooch, and Niloy J Mitra. 2009. Abstraction of man-made shapes. *ACM Trans. Graph.* 28, 5 (2009), 1–10.
- Werner Müller. 1990. *Grundlagen gotischer Bautechnik: ars sine scientia nihil*. Deutscher Kunstverlag.
- Andrew Nealen, Takeo Igarashi, Olga Sorkine, and Marc Alexa. 2007. Fibermesh: designing freeform surfaces with 3d curves. *ACM Trans. Graph.* 26, 3 (2007), 41–es.
- Günay Orbay and Levent Burak Kara. 2011. Sketch-based modeling of smooth surfaces using adaptive curve networks. In *Proceedings of the eighth eurographics symposium on sketch-based interfaces and modeling*. ACM, New York, NY, USA, 71–78.
- Hao Pan, Yang Liu, Alla Sheffer, Nicholas Vining, Chang-jian Li, and Wenping Wang. 2015. Flow aligned surfacing of curve networks. *ACM Trans. Graph.* 34, 4 (2015), 1–10.
- Hyungjun Park. 2004. Optimal single biarc fitting and its applications. *Computer-Aided Design and Applications* 1, 1-4 (2004), 187–195.
- DB Parkinson and DN Moreton. 1991. Optimal biarc-curve fitting. *Computer Aided Design* 23, 6 (1991), 411–419.
- Les A Piegl and Wayne Tiller. 2002. Data approximation using biarcs. *Engineering with computers* 18 (2002), 59–65.
- Ulrich Pinkall and Konrad Polthier. 1993. Computing discrete minimal surfaces and their conjugates. *Experimental mathematics* 2, 1 (1993), 15–36.
- Mohammed Mahbubur Rahman. 2015. Islamic architecture and arch. *International Journal of Built Environment and Sustainability* 2, 1 (2015), 8–16.
- Alec Rivers, Frédo Durand, and Takeo Igarashi. 2010. 3D modeling with silhouettes. *ACM Trans. Graph.* (2010), 1–8.
- Takafumi Saito and Tokiichiro Takahashi. 1990. Comprehensible rendering of 3-D shapes. In *Proceedings of the 17th annual conference on Computer graphics and interactive techniques*. ACM, New York, NY, USA, 197–206.
- G. D. Sandel. 1937. Zur Geometrie der Korbbgen. *Zamm-zeitschrift Fur Angewandte Mathematik Und Mechanik* 17 (1937), 301–302. <https://api.semanticscholar.org/CorpusID:119355320>
- Bruce M Savage and Michael C Johnson. 2001. Flow over ogee spillway: Physical and numerical model case study. *Journal of hydraulic engineering* 127, 8 (2001), 640–649.
- Jens Schönherr. 1993. Smooth biarc curves. *Computer Aided Design* 25, 6 (1993), 365–370.
- Lon R. Shelby. 1977. *Gothic Design Techniques: The Fifteenth-Century Design Booklets of Mathes Roriczer and Hanns Schmuttermayer*. Southern Illinois University Press, USA.
- Joe Takayama. 2024. Tracery Designer: A Metaball-Based Interactive Design Tool for Gothic Ornaments. In *SIGGRAPH Asia 2024 Posters*. ACM Digital Library, New York, NY, USA, 1–2.
- Andrew Tallon. 2014. Divining proportions in the information age. *Architectural Histories* 2, 1 (2014), 1–14.
- Paul Tanner. 1991. *Das Amerbach-Kabinett: Die Basler Goldschmiederrisse*. Öffentliche Kunstsammlung Basel, Basel, Switzerland.
- Achim Timmermann. 2009. *Real presence: sacrament houses and the body of Christ, c. 1270-1600*. Brepols, Turnhout, Belgium.
- Walter Ueberwasser. 1928–1930. Spätgotische Baugeometrie. *Öffentliche Kunstsammlung Basel 25–27 (1928–1930)*, 79–122.
- VDS. 2019. The Peace Tent. <https://city.vds.group/en/projects/architectural-objects/>
- Desmond J Walton and Dereck S Meek. 1994. Approximation of quadratic Bezier curves by arc splines. *J. Comput. Appl. Math.* 54, 1 (1994), 107–120.
- Matthew Ward. 1999. An Overview of Metaballs/Blobby Objects. *Math and Physics* (1999), 1–15.
- Baoxuan Xu, William Chang, Alla Sheffer, Adrien Bousseau, James McCrae, and Karan Singh. 2014. True2Form: 3D curve networks from 2D sketches via selective regularization. *ACM Trans. Graph.* 33, 4 (2014), 131:1–13.
- Qinwen Ye, Rong Huang, Huanhuan Liu, and Zhaohui Wang. 2023. Individualized garment pattern generation in batches based on biarc and ezdx. *AATCC Journal of Research* 10, 4 (2023), 250–262.
- Shin Yoshizawa, Alexander Belyaev, and Hans-Peter Seidel. 2005. Fast and robust detection of crest lines on meshes. In *Proceedings of the 2005 ACM symposium on Solid and physical modeling*. ACM, New York, NY, USA, 227–232.
- Emilie Yu, Rahul Arora, J Andreas Baerentzen, Karan Singh, and Adrien Bousseau. 2022. Piecewise-smooth surface fitting onto unstructured 3D sketches. *ACM Trans. Graph.* 41, 4 (2022), 1–16.
- Qingnan Zhou, Tino Weinkauff, and Olga Sorkine. 2011. Feature-Based Mesh Editing. In *Proc. EUROGRAPHICS, Short Papers*.
- Cornelis Zwicker. 2011. *The advanced geometry of plane curves and their applications*. Courier Corporation, MA, USA.

# Supplemental Materials: Computational Modeling of Gothic Microarchitecture

## A Biarcs, Ogee arcs & reverse curves

We focus on Ogee arcs (also known as reverse curves), a special subset of biarcs used to model Gothic microarchitecture. Previous studies have explored methods to determine control points for biarcs and to fit biarcs to discrete data [Meek and Walton 1992; Park 2004; Parkinson and Moreton 1991]. Additionally, the derivation of the locus of all feasible points of reverse curvature (PRCs) has been investigated [Sandel 1937].

In this section, we provide a detailed explanation of how to construct a reverse curve connecting two points,  $A$  and  $B$ , with specified tangent directions,  $\mathbf{d}_A$  and  $\mathbf{d}_B$ , respectively. According to Def. 4.1, the task involves finding two circles, centered at  $O_A$  and  $O_B$  with radii  $r_A$  and  $r_B$ , respectively, that satisfy the following conditions:

- The circle centered at  $O_A$  passes through the point  $A$  and aligns with the tangent direction  $\mathbf{d}_A$ .
- The circle centered at  $O_B$  passes through the point  $B$  and aligns with the tangent direction  $\mathbf{d}_B$ .
- The two circles intersect at an unknown point  $C$  (the PRC), where the tangents at  $C$  are parallel.

### A.1 Locus of PRCs

We begin by geometrically describing the locus of all possible PRCs of biarcs connecting a given pair of points and aligning their tangents. Sandel [1937] presented a proof in German. For completeness, we review this result and provide a detailed derivation.

**REMARK 2.** Given two points  $A$  and  $B$ , with corresponding tangent directions  $\mathbf{d}_A$  and  $\mathbf{d}_B$ , respectively, let  $D$  be the intersection point of the two tangent lines, i.e.,  $D = \mathbf{d}_A \cap \mathbf{d}_B$ . Denote the perpendicular bisector of the line segment  $AB$  as  $\ell$ . Let  $O$  be the intersection point of  $\ell$  and the circumcircle of the triangle  $\triangle ABD$ . The circular arc  $\widehat{AB}$  on the circle centered at  $O$  with radius  $\|OA\| = \|OB\|$  represents the locus of all feasible points of reverse curvature (PRC) for the reverse curves passing through points  $A$  and  $B$  with tangents  $\mathbf{d}_A$  and  $\mathbf{d}_B$  respectively.

**PROOF.** Our goal is to prove that any point  $C$  lying on this arc  $\widehat{AB}$  is a point of reverse curvature. To prove this, we need to show: (1) There exists a circle with center  $O_A$  (unknown) that passes through  $A$  and  $C$  with tangent at point  $A$  equal to  $\mathbf{d}_A$ , (2) There exists another circle with center  $O_B$  (unknown) that passes through  $B$  and  $C$  with tangent at point  $B$  equal to  $\mathbf{d}_B$ , (3) The tangents of the two circles at point  $C$  are opposite to each other. We provide the proof of construction as follows.

Denote the normals at point  $A$  and  $B$  as  $\mathbf{n}_A$  and  $\mathbf{n}_B$ , respectively, where  $\mathbf{n}_A \perp \mathbf{d}_A$  and  $\mathbf{n}_B \perp \mathbf{d}_B$ . Let  $F$  be the intersection point of the two normal lines, i.e.,  $F = \mathbf{n}_A \cap \mathbf{n}_B$ . Since  $\angle AFB = \angle ADB$ , according to inscribed angle theorem, we know that point  $F$  also lies on the circumcircle of the triangle  $\triangle ABD$ . Since point  $O$  is the intersection of the perpendicular bisector of line segment  $AB$  and the circumcircle of points  $\{A, B, F, D\}$ , we have  $\|OA\| = \|OB\|$ . Additionally,  $\angle AOB = \angle AFB = \angle ADB := \alpha$  (according to inscribed angle theorem). Since point  $C$  lies on the circle centered at  $O$  with

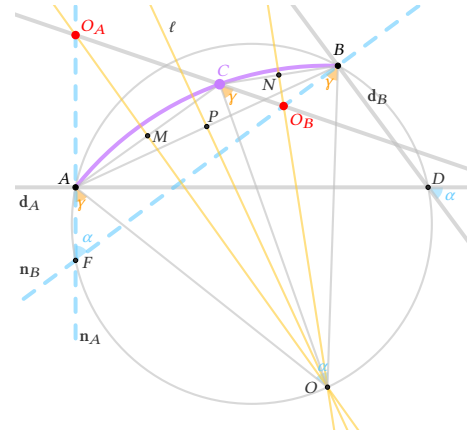


Fig. A.1. Let point  $D$  be the intersection of the tangent lines at point  $A$  and the tangent lines at point  $B$ . Denote the perpendicular bisector of line segment  $AB$  as  $\ell$ . Let point  $O$  be the intersection of  $\ell$  and the circumcircle of the triangle  $\triangle ABD$ . The arc, colored in purple, lying on the circle centered at point  $O$  with radius  $\|OA\|$ , shows the locus of all feasible points of reverse curvature (PRC). For an arbitrary point  $C$  on the arc, let  $O_A$  (or  $O_B$ ) be the intersection of the bisector of line segment  $AC$  (or  $BC$ ) and the normal lines  $\mathbf{n}_A$  (or  $\mathbf{n}_B$ ).  $O_A$  and  $O_B$  are the circle centers for the reverse curve connecting point  $A$  and  $B$  passing through the chosen point  $C$ . See Remark 2.

radius  $\|OA\|$ , we have  $\|OA\| = \|OB\| = \|OC\|$ . Let  $M$  and  $N$  be the midpoints of the line segments  $AC$  and  $BC$  respectively. Then, the lines  $OM$  and  $ON$  are the perpendicular bisector of the line segments  $AC$  and  $BC$  respectively. Denote the intersection between  $OM$  and the normal line  $\mathbf{n}_A$  as  $O_A$ , and the intersection between  $ON$  and normal line  $\mathbf{n}_B$  as  $O_B$ . By construction, we can easily see that  $\|AO_A\| = \|CO_A\|$ , and the circle centered at  $O_A$  with radius  $\|AO_A\|$  passes through point  $A, C$  with the tangent at point  $A$  equal to  $\mathbf{d}_A$ . Similarly, we have constructed the circle centered at  $O_B$  with radius  $\|BO_B\|$  passes through point  $B, C$  with tangent at point  $B$  equal to  $\mathbf{d}_B$ . Refer to Fig. A.1 for the notations used.

What remains to be shown is that the tangents of the two constructed circles at point  $C$  are opposite to each other, which is equivalent to having the three points  $O_A, C, O_B$  lying on the same line. Since  $\{A, F, B, O\}$  lie on the same circle, according to the inscribed angle theorem, we have  $\angle OAF = \angle FBO := \gamma$ . Since the triangle  $OCO_B$  and the triangle  $OBO_B$  are identical to each other, we have  $\angle OCO_B = \angle OBO_B$ . Since  $O_B$  lies on the normal lines  $BF$ , we have  $\angle OBO_B = \angle FBO = \angle OCO_B = \angle OAF = \gamma$ . Since the points  $\{O, M, O_A\}$  lie on the perpendicular bisector of the line segment  $AC$ , we have  $\angle ACO = \angle CAO$ ,  $\angle O_ACA = \angle O_AAC$ . Since the points  $\{O_A, A, F\}$  lie on the same line (the normal line at point  $A$ ), we have  $\angle O_AAC + \angle CAO + \angle OAF = \pi$ . We then have  $\angle O_ACA + \angle ACO + \angle OCO_B = \pi$ . Therefore the three points  $O_A, C, O_B$  are colinear. ■

Note that, in the special case of parallel tangents ( $\mathbf{d}_B \parallel \mathbf{d}_A$ ), the angle  $\alpha$  between  $\mathbf{d}_A$  and  $\mathbf{d}_B$  reduces to  $\alpha = 0$ . In this case, the

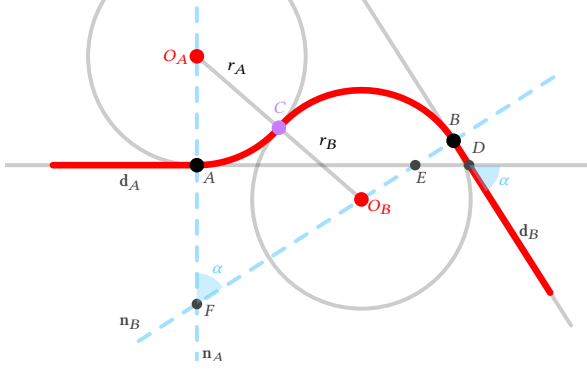


Fig. A.2. Given two points  $A$  and  $B$  with tangent directions  $\mathbf{d}_A$  and  $\mathbf{d}_B$ , respectively, a *reverse curve* connecting these points (colored in red) is composed of two circular arcs. The tangent of the reverse curve at point  $A$  (and  $B$ ) equal to  $\mathbf{d}_A$  (and  $\mathbf{d}_B$ ), with the arcs turning in opposite directions and sharing a common tangent at the intersection point  $C$  (colored in purple), known as the *point of reverse curvature* (PRC).

intersection points  $F$  and  $D$  between two parallel tangent lines and normal lines do not exist in the finite space, or can be considered to lie at infinity. Consequently, the circumcircle of point  $A, B, F, D$  degenerates into a circle of infinite radius, which becomes a straight line. The locus of the PRC therefore simplifies to an arc of this infinitely large circle, which further reduces to the line segment connecting  $A$  and  $B$ . This result is formalized in Remark 1.

## A.2 Construction of reverse curves

The proofs in Sec. A.1 already outline a geometrical method for determining the centers  $O_A$  and  $O_B$ , as well as the radii  $r_A$  and  $r_B$ , based on a chosen PRC point  $C$  from the locus. Here, we additionally provide a numerical solution for computing the points  $O_A, O_B$ , and  $C$ , along with the radius  $r_B$ , given a user-specified radius  $r_A$ . In this case, explicitly drawing the locus is not required.

We discuss the case when  $\mathbf{d}_A \nparallel \mathbf{d}_B$ , as shown in Fig. A.2. The normal directions at  $A$  and  $B$ , denoted as  $\mathbf{n}_A$  and  $\mathbf{n}_B$  and illustrated using blue dashed lines, are orthogonal to the respective tangent lines. We can easily find the intersection points  $D = \mathbf{d}_A \cap \mathbf{d}_B$ ,  $E = \mathbf{d}_A \cap \mathbf{n}_B$ ,  $F = \mathbf{n}_A \cap \mathbf{n}_B$ , and the angle of intersection  $\alpha = \langle \mathbf{d}_A, \mathbf{d}_B \rangle$ . The distances between the points  $\{A, B, D, E, F\}$  can be easily computed. Our goal is to find the location of the centers  $O_A, O_B$  and the intersection point  $C$ . From the first two constraints, we can conclude that  $O_A$  and  $O_B$  lie on the normal directions  $\mathbf{n}_A$  and  $\mathbf{n}_B$ . We then have  $\|O_B C\| = \|O_B B\| = r_B$ ,  $\|O_A C\| = \|O_A A\| = r_A$ ,  $\|FO_B\| = \|FB\| - r_B := s - r_B$ ,  $\|FO_A\| = \|AF\| + r_A := t + r_A$ . According the third constraint that the two circles intersect at  $C$  with opposite tangents at that point, we can conclude that  $O_A, O_B, C$  lie on the same line. We then have  $\|O_A O_B\| = r_A + r_B$ . Applying the law of cosines on the triangle  $\Delta FO_A O_B$ , we have:

$$\begin{aligned} \|O_A O_B\|^2 &= \|FO_A\|^2 + \|FO_B\|^2 - 2 \|FO_A\| \|FO_B\| \cos \alpha \\ \implies (r_A + r_B)^2 &= (s - r_B)^2 + (t + r_A)^2 - 2(s - r_B)(t + r_B) \cos \alpha, \end{aligned}$$

which gives the relation between the unknown radii  $r_A$  and  $r_B$  (note  $s, t, \alpha$  are known values). Users can choose the radii  $(r_A, r_B)$  that

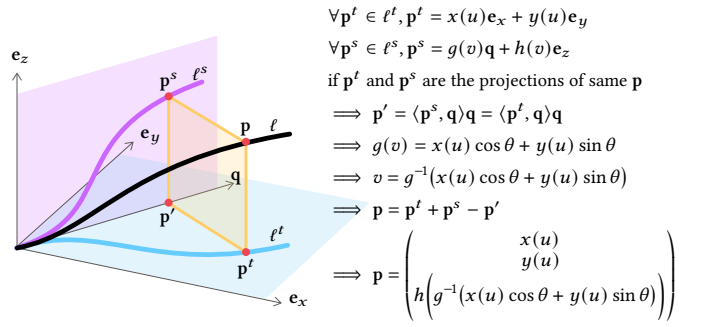


Fig. A.3. Parameterization of 3D curve  $\ell$  using its projections from the top view and side view, i.e. 2D curves  $\ell^t$  and  $\ell^s$ .

satisfy the equation and then easily derive the position of  $O_A, O_B, C$ :

$$\begin{aligned} \mathbf{O}_A &= \mathbf{A} + r_A \mathbf{n}_A, & \mathbf{O}_B &= \mathbf{B} + r_B \mathbf{n}_B, \\ \mathbf{C} &= \frac{r_B}{r_A + r_B} \mathbf{O}_A + \frac{r_A}{r_A + r_B} \mathbf{O}_B, \end{aligned}$$

where  $\mathbf{X}$  denotes the 2D positions of the point  $X$ , and normal directions can be obtained by  $\mathbf{n}_A = \frac{\mathbf{A}-\mathbf{F}}{\|\mathbf{A}-\mathbf{F}\|}$ ,  $\mathbf{n}_B = \frac{\mathbf{B}-\mathbf{F}}{\|\mathbf{B}-\mathbf{F}\|}$ .

## B Parametric curves from top & side views

Here, we provide the full details for the curve parameterization using its top and side views discussed in Sec. 4.4. Let  $\mathbf{e}_x, \mathbf{e}_y, \mathbf{e}_z \in \mathbb{R}^3$  be the unit vectors parallel to the  $x, y, z$ -axes, respectively. Let  $\mathbf{q}$  be an arbitrary unit vector on the  $xy$ -plane:  $\mathbf{q} = (\cos \theta, \sin \theta, 0)^\top$ ,  $\theta \in [0, 2\pi]$ . For a 3D curve, we obtain its top-view projection onto the  $xy$ -plane (spanned by  $\mathbf{e}_x$  and  $\mathbf{e}_y$ ) and its side-view projection onto the vertical plane spanned by  $\mathbf{q}$  and  $\mathbf{e}_z$ . More specifically, given a 3D curve parameterized by  $r$ :

$$\ell(r) = \begin{pmatrix} x(r) \\ y(r) \\ z(r) \end{pmatrix}, \quad r \in [0, 1], \quad (\text{B.1})$$

we can easily find the top-view and side-view parameterization via inner products with  $\{\mathbf{e}_x, \mathbf{e}_y\}$  and  $\{\mathbf{q}, \mathbf{e}_z\}$ :

$$\ell^t(r) = \begin{pmatrix} x(r) \\ y(r) \end{pmatrix}, \quad \ell^s(r) = \begin{pmatrix} x(r) \cos \theta + y(r) \sin \theta \\ z(r) \end{pmatrix}, \quad (\text{B.2})$$

where  $\ell^t(r)$  and  $\ell^s(r)$  denote the 2D top- and side-view projection.

Now we assume the 2D curve from the top and side view is given:

$$\ell^t(u) = \begin{pmatrix} x(u) \\ y(u) \end{pmatrix}, \quad \ell^s(v) = \begin{pmatrix} g(v) \\ h(v) \end{pmatrix}, \quad u, v \in [0, 1] \quad (\text{B.3})$$

The goal is to reconstruct the 3D curve  $\ell$  such that its top and side views are identical to  $\ell^t$  and  $\ell^s$ , respectively. From (B.2), we know that the variables of  $v, u$  need to satisfy  $g(v) = x(u) \cos \theta + y(u) \sin \theta$ , then we can reconstruct the 3D curve as:

$$\ell(u) = \begin{pmatrix} x(u) \\ y(u) \\ h\left(g^{-1}(x(u) \cos \theta + y(u) \sin \theta)\right) \end{pmatrix}, \quad u \in [0, 1] \quad (\text{B.4})$$

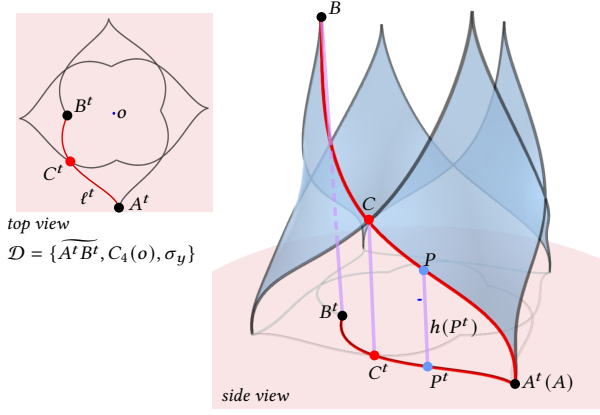


Fig. B.4. Parameterizing the side-view projection using the arc length of the top-view curve enables view-independent reconstruction.

We can easily verify the top and side view of this constructed curve  $\ell$  align with the given  $\ell^t$  and  $\ell^s$ . In Fig. A.3 we show a geometric interpretation of the proof.

In other words, instead of parameterizing a 3D curve using three functions defined on a single variable as in the standard way (see Eq. (B.1)), we choose to use four functions  $x(u), y(u), h(v), g(v)$  defined on two dependent variables  $v, u$  satisfying  $g(v) = x(u) \cos \theta + y(u) \sin \theta$  (see Eq. (B.4)). In this parameterization, if we only change the shape of  $x(\cdot), y(\cdot)$  (i.e., change the projection in the top view), the side view of the 3D curve w.r.t. the angle  $\mathbf{q}$  will remain unchanged. Similarly, if we only change the shape of  $h(\cdot), g(\cdot)$  (i.e., change the projection in the side view), the top view will remain unchanged.

Note that the 3D reconstruction depends on the choice of the vertical plane for parameterizing the side-view projection, or more precisely, on the selection of  $\mathbf{q}$ . When the top-view projection consists of line segments only, it is natural to choose  $\mathbf{q}$  that aligns with the basic curve in the top-view, which results in the side-view projection lying on the vertical plane that extends from the top-view drawing. We can further make the parameterization in Eq. (B.4) to be *view-independent* (i.e., independent on the choice of  $\mathbf{q}$ ) by defining the function  $g(v)$  as the arc-length of the top-view drawing:

$$g(v) = \int_0^v \sqrt{x'(u)^2 + y'(u)^2} du. \quad (\text{B.5})$$

This formulation can be interpreted as projecting the 3D curve onto a ruled surface (not necessarily a vertical plane) extending from the top-view curve (see Fig. B.4), and  $h(\cdot)$  in Eq. (B.4) serving as a height function. Notably this construction is view-independent.

### C User interface & algorithmic details

We developed a web-based user interface using JavaScript for interactive modeling and editing for Gothic microarchitecture. The main functions include:

- Specify the rotational and reflectional symmetries.
- Draw basic curves using line segments or circular arcs.
- Load historical 2D drawings, where the basic curves and symmetries have been identified (e.g., see Figures C.5 and C.6).

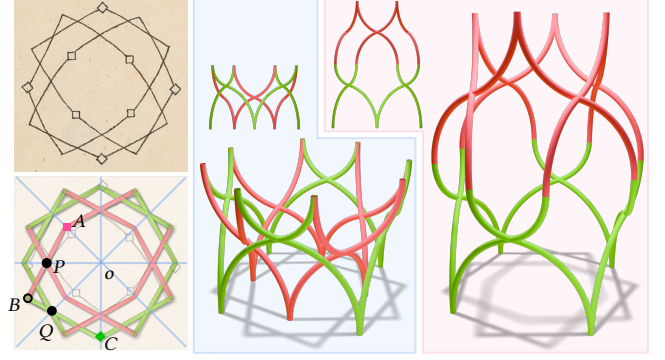


Fig. C.5. *Top left*: Inv.U.XI.26, 10.4 × 15.3 cm. Image source: Kunstmuseum Basel (Public Domain). *Bottom left*: its top-view representation  $\mathcal{D} = \{\overline{AB} \cup \overline{BC}, C_4(o), \sigma_y\}$ . The two basic curves and their corresponding replicas are colored in red and green respectively. Following Algo. 1 we determine the PRC for the two basic curves, denoted as point  $P$  and  $Q$  respectively. *Middle & right*: By assigning different heights to the marked vertices (point  $A$  and  $C$ ) we can generate various designs, where we show both side and 3D view.

---

#### ALGORITHM 1: Determining Points of Reverse Curvature (PRC)

---

**Data:** top view drawing  $\mathcal{D}^t = \{\mathcal{L}^t, C_n(\mathbf{p}), \sigma_d\}$

**Result:** PRC for each basic curve  $\ell \in \mathcal{L}^t$

**for each basic curve**  $\ell \in \mathcal{L}^t$  **do**

    find intersections between  $\ell$  and its replicas;

**if such intersections are found then**

        | **return** the one closest to the midpoint of  $\ell$  as PRC;

**else**

        Find intersections between  $\ell$  and the other distinct basic curves and their replicas;

**if such intersections are found then**

            | **return** the one closest to the midpoint of  $\ell$  as PRC;

**else**

            | **return** the midpoint of  $\ell$  as PRC;

**end**

**end**

**end**

---

- Automatically complete the full top-view projection using the specified symmetries.
- Automatically detect the point of reverse curvature (PRC) for each basic curve using Algorithm 1.
- Automatically compute the 3D curve by fitting biarcs to the side view using the detected PRC. For open-ended curves, a biarc is fitted to its first arc, while the second arc descends from the ceiling point to a midpoint with free end (e.g. see Fig. 9 (g,h,i)).
- Edit the shape in the top view or side view, and automatically update the 3D curves.
- Change PRC by clicking on some intersection point from the top view and automatically update the 3D curves.
- Add decorations to selected arcs: The selected arc and its replicas are split into two arcs of equal radius while maintaining their top-view projections and endpoint tangents. See Fig. C.8.
- Create multi-layer drawings or convert a single-layer drawing into a multi-layer structure.

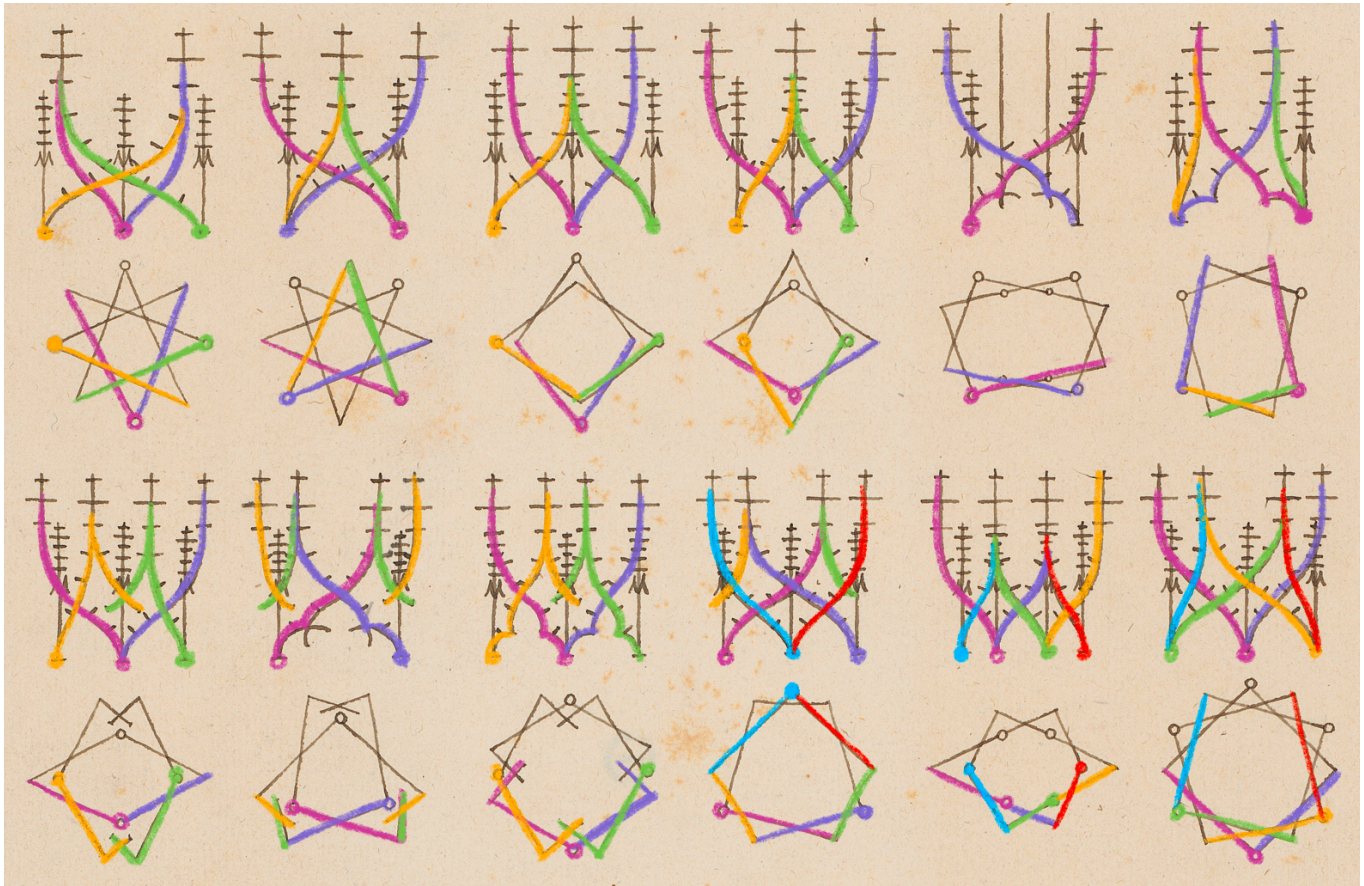


Fig. C.6. For the examples shown in the teaching notes 'U.XI.11,' shown in Fig. 5, we use consistent colors to highlight the corresponding curves in the top views (second and fourth rows) and side views (first and third rows).

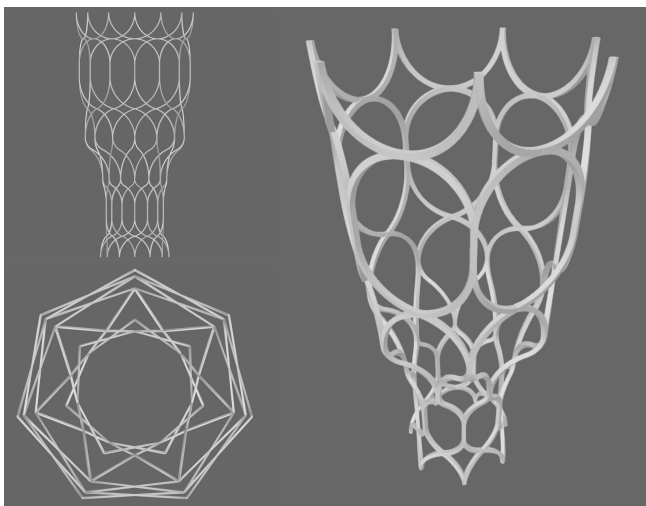


Fig. C.7. Screenshot of using our UI modeling the Gothic chancel shown in Fig. 13. In *preview* mode, the UI displays the 3D view using a perspective camera, along with the top and side views using an orthographic camera.

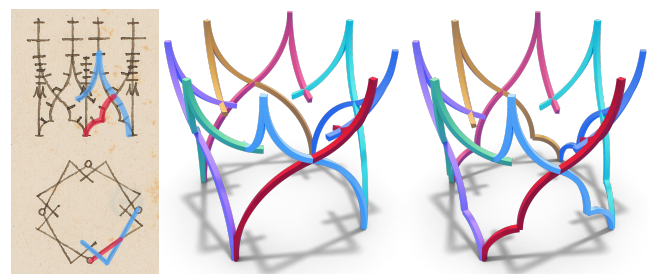


Fig. C.8. *Left*: "U.XI.11"(2,3) features a top-view drawing with open-ended curves (highlighted in blue) and a side-view drawing where the lower part of the biarc splits into two decorative arcs (highlighted in red). Our reconstructions (*right* and *middle*) compare variants with and without the decorative arcs.

- Fill the minimal-area face for a selected curve loop based on [Pinkall and Polthier 1993].
- Switch the visualization to curve mode or ribbon mode.
- Switch between design mode and preview mode (as shown Fig. C.7).
- Save and load the user's design.
- Export the user's design in different styles as a ".obj" file.